

# A superconducting nanowire single-photon detector system for single-photon source characterization

C. R. Fitzpatrick<sup>1,2</sup>, C. M. Natarajan<sup>1</sup>, R. E. Warburton<sup>1</sup>, G. S. Buller<sup>1</sup>,  
B. Baek<sup>3</sup>, S. Nam<sup>3</sup>, S. Miki<sup>4</sup>, Z. Wang<sup>4</sup>, M. Sasaki<sup>4</sup>, A. G. Sinclair<sup>2</sup>, R. H. Hadfield<sup>1</sup>

1. Heriot-Watt University, Edinburgh, UK,

2. National Physical Laboratory (NPL), Teddington, UK,

3. National Institute of Standards and Technology (NIST), Boulder, USA,

4. National Institute of Information and Communications Technology (NICT), Japan

## ABSTRACT

Single-photon sources and detectors are key enabling technologies for photonics in quantum information science and technology (QIST). QIST applications place high-level demands on the performance of sources and detectors; it is therefore essential that their properties can be characterized accurately. Superconducting nanowire single-photon detectors (SNSPDs) have spectral sensitivity from visible to beyond 2  $\mu\text{m}$  in wavelength, picosecond timing resolution (Jitter <100 ps FWHM) and the capacity to operate ungated with low dark counts (<1 kHz). This facilitates data acquisition at high rates with an excellent signal-to-noise ratio.

We report on the construction and characterization of a two-channel SNSPD system. The detectors are mounted in a closed-cycle refrigerator, which eliminates reliance on liquid cryogenics. Our specification was to deliver a system with 1 % efficiency in both channels at a wavelength of 1310 nm with 1 kHz dark count rate. A full width at half maximum timing jitter of less than 90 ps is achieved in both channels. The system will be used to detect individual photons generated by quantum-optical sources at telecom wavelengths. Examples include single-photon sources based on quantum dots (emitting at 1310 nm). The SNSPD system's spectral sensitivity and timing resolution make it suited to characterization of such sources, and to wider QIST applications.

**Keyword list:** quantum information, quantum optics, single-photon detector, single-photon source, superconducting detector

## 1. INTRODUCTION

The emerging field of quantum information science and technology (QIST)<sup>[1]</sup> would benefit greatly from the development of high-performance single-photon sources<sup>[2]</sup> and detectors<sup>[3]</sup>. Despite impressive progress, the properties of current single-photon devices do not meet the stringent demands of high-level applications such as linear optical quantum computing<sup>[4]</sup>. The variation in performance requirements across QIST applications makes the realization of a 'one size fits all' system for single photons highly unlikely.

High-performance sources and detectors at telecom wavelengths are crucial to the development of viable fiber-based systems. III-V semiconductor quantum dots are leading candidates for single-photon generation at 1.3  $\mu\text{m}$ <sup>[2,5]</sup>. This is beyond the spectral range of silicon single-photon avalanche photodiodes (SPADs)<sup>[6]</sup>. InGaAs SPADs have single

photon sensitivity at telecom wavelengths but suffer from high dark count rates and require gating [7]. Superconducting nanowire single-photon detectors (SNSPDs) have emerged as a promising alternative [8]. These detectors offer free-running single-photon detection at telecom wavelengths, combined with low dark counts and picosecond timing resolution. Their operating temperature ( $\sim 4\text{K}$ ) can be attained by the use of a closed-cycle refrigerator system [9].

In this paper we report on the construction of a practical SNSPD detector system that is well suited to quantum optics experiments at telecom wavelengths. The principle of operation, characterization and construction of the system, and planned experiments, will be described.

### 1.1 Device focus: Superconducting Nanowire Single-Photon Detectors (SNSPDs)

Single photon detection with superconducting niobium nitride (NbN) nanowires was first demonstrated by Gol'tsmann et al. in 2001 [8]. The detection mechanism is based on 'hot spot formation' – the localised breaking of Cooper pairs in the nanowire by an incident photon (represented in Figure 1). If the diverted super-current exceeds the critical current density, a resistive bridge forms temporarily across the width of the nanowire. A measurable voltage pulse is produced as a consequence of the incident photon.

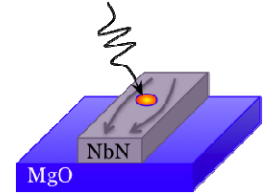


**Figure 1:** Illustration of 'hot spot' formation on a nanowire

The energy gap between the superconducting and normal ground states is  $\sim \text{meV}$ . This results in single-photon sensitivity in superconductors at longer wavelengths than the most commonly employed semiconductors, which are limited by a bandgap energy of the order  $\sim \text{eV}$ . The spectral range of SNSPDs has been reported to extend as far as  $5.6\ \mu\text{m}$  [10]. Additionally, SNSPDs have picosecond timing resolution (jitter  $< 100\ \text{ps}$  FWHM) and the capacity to operate ungated with low dark counts ( $< 1\ \text{kHz}$ ), which facilitates data acquisition at high rates with excellent signal-to-noise.

Currently, practical detection efficiency is a limiting factor for SNSPDs. The SNSPD devices used in this study are based on a meander design [11, 12], where the nanowire is folded back on itself to cover a large area. This makes it suitable for coupling with single mode optical fiber. Devices of this type have been reported with 2 % system detection efficiency at  $1550\ \text{nm}$  with  $100\ \text{Hz}$  dark counts [12]. Recent work has shown that there is considerable scope for improvements in efficiency with cavity-enhanced nanowire designs [13, 14]. The current properties and potential for future advancement make SNSPDs an attractive prospect as an enabling technology in QIST.

## 2. SNSPD SYSTEM DESCRIPTION

### 2.1 Cooling setup and electrical connections

The SNSPD system comprises a custom-built cryostat that contains two fiber-coupled nanowire samples, referred to hereafter as channels A and B. The nanowires are etched in a meander pattern into a  $4\ \text{nm}$  thin film of NbN on a single-crystal MgO substrate. The wires are  $100\ \text{nm}$  wide and cover a  $20\ \mu\text{m} \times 20\ \mu\text{m}$  area with a 50 % fill factor. The samples were fabricated by S. Miki et al. at NICT, Japan [12].

Use of a Gifford-McMahon cryocooler eliminates the need for liquid cryogenics and provides sufficient cooling power for multiple chips in the same cryostat [9]. Silicon diode temperature sensors monitor the system temperature at the first and second cooling stages of the cold head, and at an additional stand-off stage where the chips are mounted. The stand-off stage is mounted on the cold head, on top of a lead puck (see photograph in Figure 2 (left)). The heat capacity of the lead increases the thermal time constant of the stand-off stage, which improves the temperature stability of the packaged nanowire devices. The electrical signal is transported from the cold stage to room temperature by use of brass coaxial cable. This material was chosen for its high electrical and low thermal conductivity. Low-noise high-speed amplifiers are placed just outside the cryostat, at room temperature. This was considered to be the most suitable arrangement, due to the additional heat load that low-temperature amplifiers would introduce.

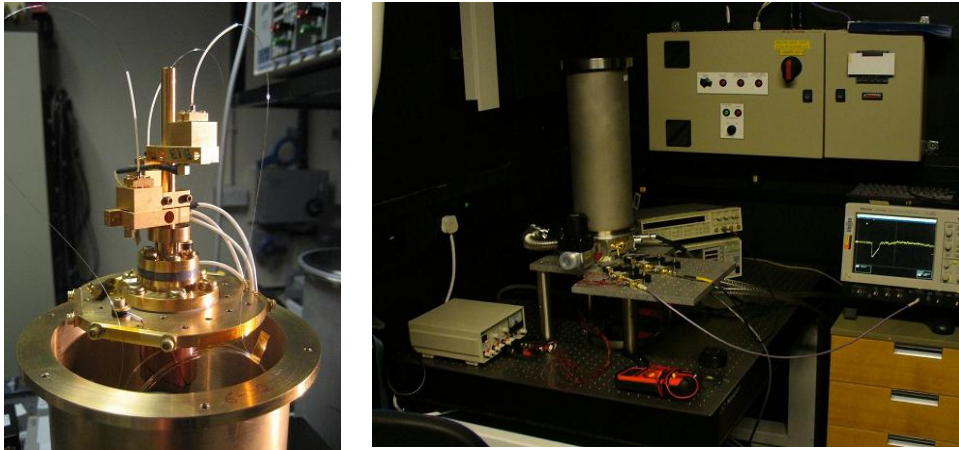


**Figure 2:** (left) Photograph of packaged samples mounted on the cold head of the SNSPD system; (right) Photograph of the SNSPD system operating at NPL.

## 2.2 Optical alignment

A scanning electron micrograph of a nanowire sample is shown in Figure 3 (right). The ideal fiber position in the x-y plane centres the beam spot on the active nanowire meander. Optimal coupling is achieved by adjusting the fiber-chip distance to match the beam diameter with the meander area. The distance between the end of the fiber and the chip was adjusted by the use of a selection of shims, and measured with white light interferometry, using the interference between reflections from the two surfaces<sup>[15]</sup>. A fiber-chip separation of 25  $\mu\text{m}$  to 40  $\mu\text{m}$  at  $T = 3\text{ K}$  was achieved. The optical fiber and the nanowire chip are secured to separate halves of a custom-made sample mount, to allow x-y alignment independently of the fiber-chip distance. The beam spot on the chip is observed by coupling infrared laser light into the fiber, and viewing the reverse side of the chip with an infrared camera. This is shown in Figure 3 (left), where the spot position can be observed relative to key features on the chip. These features are visible due to broad illumination of the chip, and provide a guide for the x-y alignment.

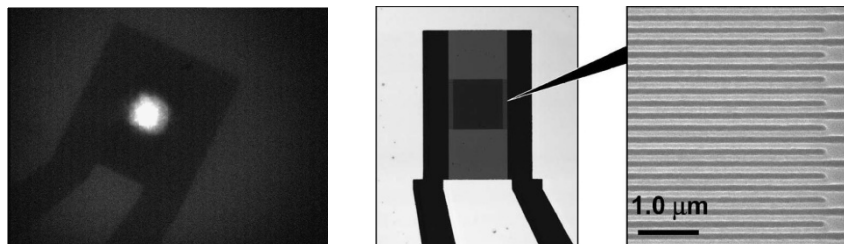


**Figure 3:** (left) x-y alignment – the beam spot from the fiber is aligned to be centered on the active nanowire area; (right) the placement of the active area relative to the outline of the chip is shown, with a scanning electron micrograph image of the nanowires (Source: S. Miki et. al, APL 92 061116 (2008)).

## 3. SNSPD SYSTEM CHARACTERIZATION

### 3.1 Current-voltage characteristics & output signal

The superconducting critical current of a NbN nanowire is determined from its current-voltage (I-V) characteristic. Detection efficiency can be maximised by applying a current bias just below the critical current. If a device has a lower than expected critical current, this may indicate the presence of constrictions in the nanowire<sup>[16,17]</sup>. Constrictions limit the maximum bias that can be applied to the device, which reduces the maximum detection efficiency. Figure 4 shows I-

V data for channel A. Data were compiled by measuring the voltage across the device at a range of bias currents. A clear switch to classical ohmic behaviour is observed at the critical current. The critical currents for channels A and B were measured to be 17  $\mu\text{A}$  and 15  $\mu\text{A}$  respectively. Values up to 20  $\mu\text{A}$  were recorded for similar devices at the same operating temperature<sup>[15]</sup>.

Typical SNSPD output pulses have a magnitude of 250-300 mV, a 4 ps leading edge and a 10 ns recovery period. Figure 4 (right) is a recorded trace of such a pulse. The magnitude of the output is directly compatible with the trigger input of a time-correlated single-photon counting module. The leading edge of the pulse is discriminated to obtain accurate timing information, while the 10 ns recovery period permits a maximum count rate of 0.1 GHz.

Figure 5 includes a circuit diagram of the detector system. A current bias is applied to the nanowire by use of a voltage source in series with a 100 k $\Omega$  resistor. This is supplied through the DC arm of a bias tee, while the fast output pulses are amplified via a room-temperature high-speed amplifier chain and read out from the AC arm of the bias tee. A 50  $\Omega$  shunt resistor in parallel with the nanowire device provides a passive reset mechanism. As the resistance in the triggered nanowire increases, more of the current flows through the shunt resistor, which allows the nanowire to return to its superconducting state.

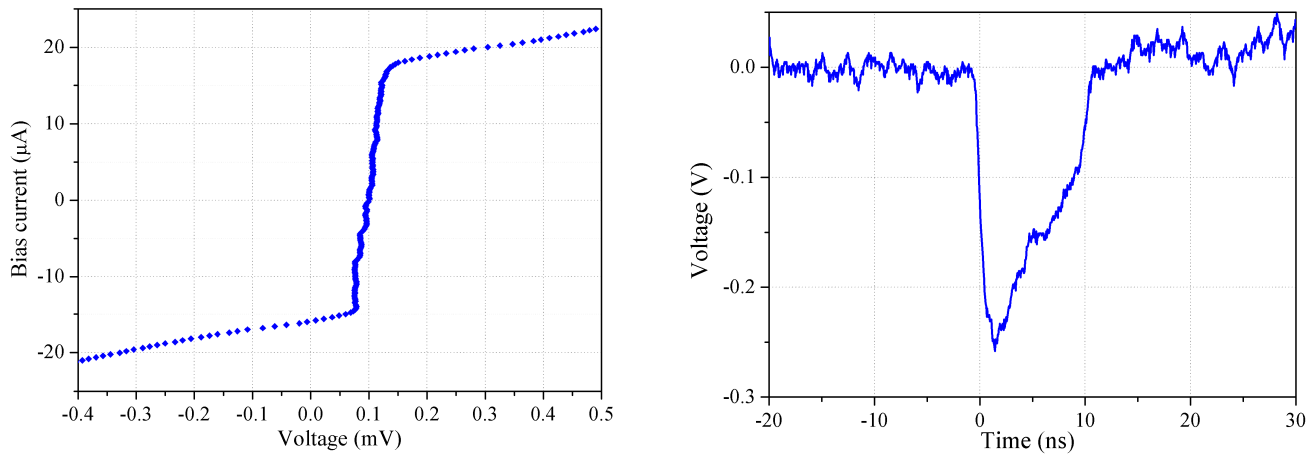


**Figure 4:** (left) I-V characteristics data for channel A of the SNSPD system. The critical current is 17  $\mu\text{A}$ ; (right) A typical SNSPD output pulse. The fast leading edge provides the low timing jitter, while the 10 ns recovery period accommodates count rates up to 0.1 GHz. The pulse shown is a ‘dark count’, which has the same form as pulses produced by incident photons.

### 3.3 System detection efficiency

The system detection efficiency was measured for both channels by use of the calibrated light source method<sup>[3]</sup>. Figure 5 (left) is a schematic of the setup used for this measurement. Highly attenuated laser pulses were produced using a gain-switched laser diode in series with calibrated optical attenuators with a dynamic range of 0 dB to 120 dB. Figure 5 (right) shows the recorded count rate as a function of photon flux for three bias currents. The data are described by

$$R = D + f(1 - e^{-\eta\mu}), \quad (1)$$

where  $R$  is the count rate,  $D$  is the ungated dark count rate,  $f$  is the laser pulse rate,  $\mu$  is the average number of photons per pulse and  $\eta$  is the system detection efficiency, including optical coupling losses<sup>[3,9]</sup>. The use of a pulsed source ensures the data are not affected by device dead time, and provides a fixed saturation point at the pulse repetition rate. The pulse duration was set to match the recovery time of the detector (10 ns), to prevent multiple consecutive detection events occurring due to the same pulse. Single photon detection is evidenced by an order of magnitude increase in photon flux causing in an order of magnitude increase in detection rate. The count rate versus photon flux data of Figure 5 (right) can be fitted using equation (1) to extract system detection efficiency as a function of dark count rate: data for the wavelengths 830 nm, 1310 nm and 1550 nm is shown in Figure 6.

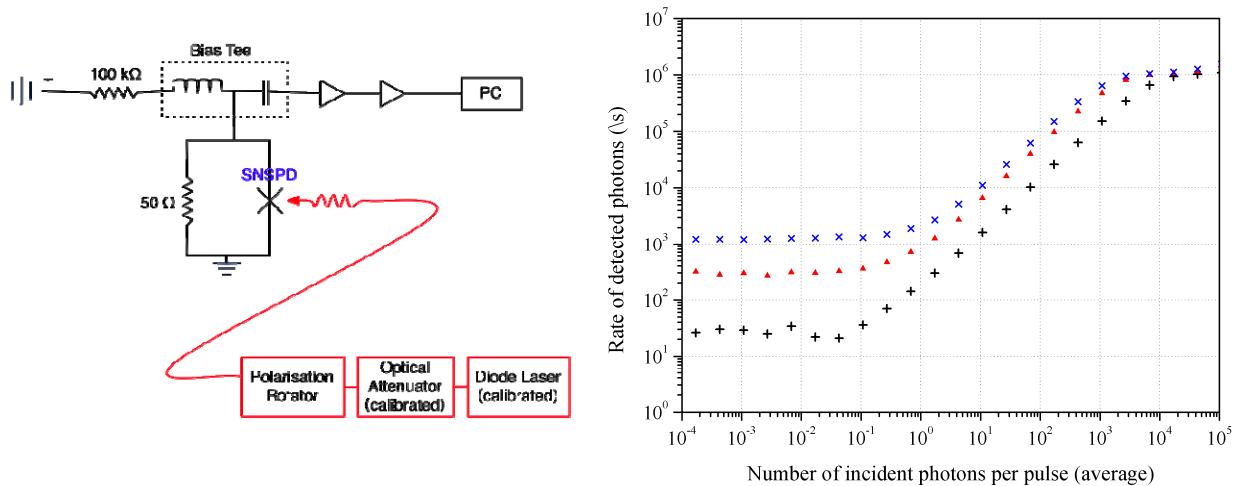


**Figure 5:** (left) Schematic of experimental setup for measurement of system detection efficiency. The calibration of the diode laser and programmable attenuators allows the calculation of absolute optical power delivered; (right) Raw measurement data – Recorded count rate as a function of the number of incident photons per pulse. The data shown are recorded at three different current bias points (+) lowest bias, (x) highest bias. The detector was illuminated with a gain-switched diode laser with 1MHz frequency and 10 ns pulse duration.

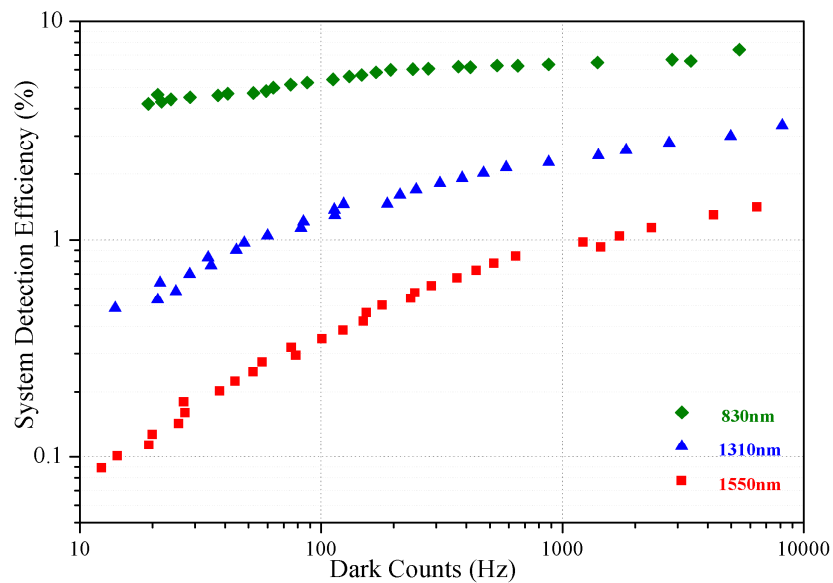


**Figure 6:** System detection efficiency measurements for SNSPD channel A at 830 nm, 1310 nm and 1550 nm. Data were recorded at a range of bias currents to yield information on the relationship between efficiency and dark count rate. Data measured at a device operating temperature of 2.6 K.

### 3.4 Timing jitter

Timing jitter ( $\Delta t$ ) is a key performance characteristic for a single-photon detector. It determines how accurately photon arrivals can be time-stamped or gated, eliminating the effects of dark counts. Figure 7 is a schematic of the jitter measurement setup, based on the time-correlated single-photon counting technique. A diode laser is driven by a pulse pattern generator (PPG), which enables an electrical reference signal to be correlated with output pulses from the

detector. A low-jitter PPG and laser setup was used (<50 ps FWHM) so that the SNSPD was the dominant source of timing jitter. Gaussian fits to the jitter data for detector channels A and B gave values of 84 ps FWHM and 88 ps FWHM respectively; the data and fit for channel B are shown in Figure 7.

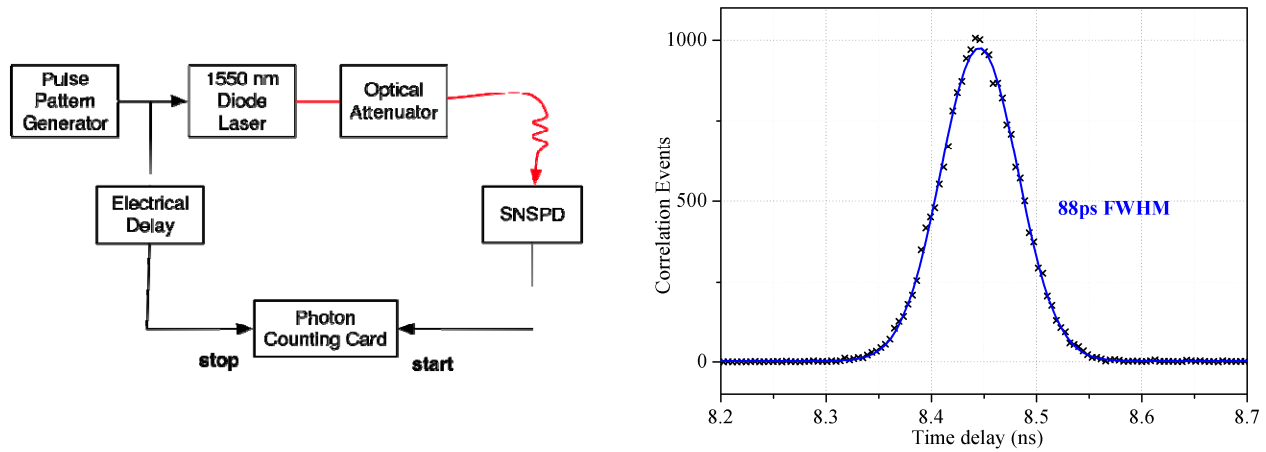


**Figure 7:** (left) Schematic diagram of experimental setup for jitter measurements; (right) correlation data for channel B; the timing jitter of the system is 88 ps FWHM, with the SNSPD being the dominant source of jitter in the experiment.

### 3.5 Summary of SNSPD system characterization measurements

The performance of the two SNSPD channels in our current system is summarised in Table I. At  $\lambda = 1310$  nm with a 1 kHz dark count rate, practical detection efficiencies of 2.2 % and 1 % were measured in channels A and B, respectively. The operating temperature of the devices is 2.6 K. This performance is somewhat lower than the best results for this type of device under similar optical coupling conditions and operating temperature reported in Refs [12,15]. However, our system meets the target specification of 1 % practical efficiency in both channels at 1310 nm wavelength at 1 kHz dark count rate.

Detector Channel	Critical current	Detection efficiency $\eta$ at 1 kHz dark count rate			Timing jitter $\Delta t$
		830 nm	1310 nm	1550 nm	
A	17 $\mu$ A	6 %	2.2 %	1 %	84 ps FWHM
B	15 $\mu$ A	5.5 %	1 %	0.3 %	88 ps FWHM

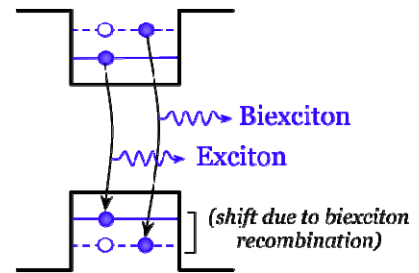
**Table 1:** Summary of SNSPD detector system properties

## 4. QUANTUM DOT SINGLE-PHOTON SOURCES

Single-photon sources are a fundamental component in optical QIST applications. They have been comprehensively reviewed in recent literature [18,19], and include systems based on quantum dots [20], single trapped ions [21] and nitrogen vacancy centers in diamond [22]. The use of SNSPD systems to characterize quantum-dot single-photon sources (QD SPS) has been demonstrated [9,23,24] – we plan to extend this work with our newly constructed SNSPD system.

## 4.1 Device concept

A quantum dot is a small amount of one type of semiconductor, completely surrounded by a semiconductor with a larger band gap. The difference in band gap energies creates a confinement potential, which causes quantization of the electron density of states (illustrated in Figure 8). Consequently, an excited quantum dot relaxes via photon emission at discrete wavelengths. These wavelengths correspond to specific transitions between states in the dot potential. The spectral selection of a single transition creates a source of single photons, because the system must be re-excited before it can undergo the same transition.



The emission from a quantum dot, which is into  $4\pi$  solid angle in bulk material, can be enhanced along one axis by placing it in a cavity, as this alters the density of modes surrounding the dot. Micropillar cavities are fabricated by etching pillars into a sample that has distributed Bragg reflectors grown on both sides of the region of interest. The dot emission and cavity wavelengths vary differently with temperature, due to the dot and surrounding material having different thermal expansion coefficients. Consequently, the system can be temperature-tuned to a point where there is coupling between the cavity and dot modes. This enhances the rate of emission from the dot via the Purcell effect; the increased mode density caused by the coupling causes a decrease in the spontaneous emission lifetime<sup>[25]</sup>.

**Figure 8:** Schematic illustration of quantum dot confinement potential, and the electron-hole recombination events that give rise to exciton and biexciton emission.

## 4.2 Characterization measurements

A setup for producing a source of single photons from a quantum dot is shown in Figure 9. A pump laser with a shorter wavelength than that of the dot emission is directed to the quantum dot sample using a long-pass filter. The emission from the dot then passes straight through the filter into a 0.5 m focal length spectrometer, which is used both to view the emission spectrum on an electron-multiplying CCD camera, and to select the exciton line with a narrow band-pass slit.

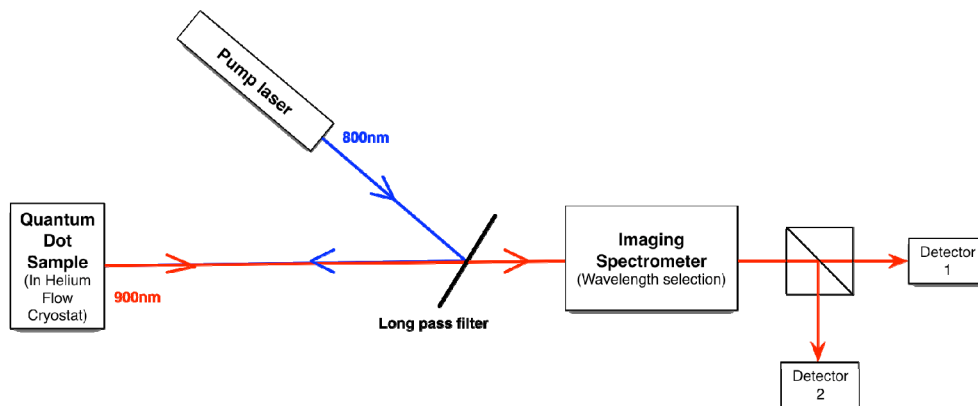


**Figure 9:** Schematic of setup used to measure the second-order correlation function,  $g^{(2)}(\tau)$  of a quantum-dot single photon-source. The pump light incident on the dot sample is separated from the emitted photons using a long pass filter. The imaging spectrometer is used to spectrally select a single transition, producing a single-photon source. The photons are then directed to a Hanbury Brown and Twiss interferometer in order to measure the second-order correlation function.

It is essential to be able to quantify how reliably such a source emits single photons. This is usually measured by the use of a Hanbury Brown and Twiss interferometer<sup>[26]</sup>, shown schematically in Figure 9. The source emission is directed towards a beam-splitter that is set up to have a single photon detector on each port. If each emitted pulse contains only one photon, it cannot be registered simultaneously on both detector channels. The histogram of detector coincidences

versus time delay,  $\tau$  gives the second order correlation function of the source,  $g^{(2)}(\tau)$ . For a true single photon source the measured coincidences will drop to zero at zero time delay (i.e. the ratio of coincidences in the  $\tau = 0$  peak to the mean ratio of coincidences in a  $\tau \neq 0$  peak,  $g^{(2)}(0) = 0$ ). This effect is shown in Figure 10, where the absence of a peak at  $\tau = 0$  corresponds to a value  $g^{(2)}(0) = 0.13 \pm 0.05$ . The measurement was made on a quantum dot embedded in a micropillar cavity with  $Q \sim 1350$ . It was optically excited with a modelocked Ti:Sapphire laser at  $\lambda = 802$  nm and the exciton emission wavelength ( $\lambda = 906$  nm) was selected. Silicon SPADs were used at each arm of the beam splitter.

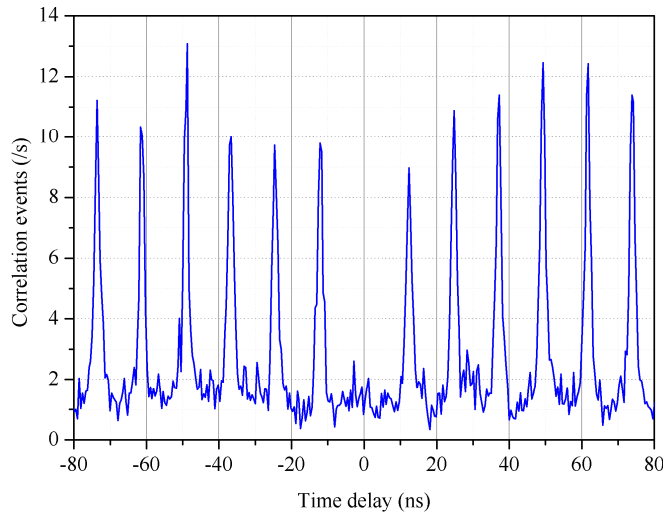


**Figure 10:** Histogram of correlation events as a function of time delay for a quantum-dot single-photon source at  $\lambda = 906$  nm measured with twin Si SPADs. This gives the second-order correlation function of the source; the result  $g^{(2)}(\tau = 0) = 0.13 \pm 0.05$  demonstrates that the source is emitting single photons. The integration time for the displayed data was 15 hrs, with a total count rate on both APDs of 1.1 kHz and timing bin width equal to 0.445 ns.

Another important characteristic of single-photon sources is the photoluminescence (PL) lifetime. This is measured using a similar setup to that used for jitter measurement (see Fig. 7). Correlating detection events from a single-photon source with an electrical signal that is triggered by the pump signal produces a peak from which the PL lifetime can be determined. The raw data is a convolution of the instrument response function (IRF) of the detector and the lifetime of the source. The Gaussian IRF of the SNSPD simplifies the deconvolution of the IRF from the data, which is necessary to extract a lifetime value<sup>[24]</sup>.

### 4.3 Suitability of SNSPD for QD SPS characterization

The setup for characterizing single-photon sources is currently being extended to facilitate operation at  $\lambda = 1310$  nm. At this wavelength, the two channels of the new SNSPD system will be used for detection at the two beam-splitter ports of the Hanbury Brown & Twiss interferometer (shown schematically in Figure 9). The properties of the SNSPD in comparison with Si SPADs (at  $\lambda \sim 900$  nm) and InGaAs SPADs (at  $\lambda \sim 1310$  nm) are shown in Table 2. The detector performance is shown in terms of detection efficiency ( $\eta$ ), dark count rate (D), timing jitter ( $\Delta t_{\text{Detector}}$ ) and also the clock rate permitted for a pulsed excitation QD SPS experiment. A figure of merit quantifying the signal to noise of the detector is also given. The signal-to-noise ratio of a detector in a time-correlated single-photon counting experiment<sup>[3]</sup> can be formulated as follows:

$$\text{Signal-to-noise ratio} = \eta / (D\Delta t) . \quad (2)$$

This figure of merit gives an indication of the extent to which the effect of the dark-count rate can be mitigated by time-stamping or binning. The minimum gating or binning interval is usually set by the jitter of the detector,  $\Delta t_{\text{Detector}}$ . It should be noted (as illustrated in Figure 6 and in Table 2) that as the bias on the SNSPD is lowered, the signal to noise

ratio improves. Therefore, in a coincidence-type measurement with SNSPDs there will be a trade-off between accumulation rate and high signal-to-noise ratio. In a QD SPS characterization experiment, however, the full impact of the low timing jitter of the SNSPD on the signal-to-noise may be lost: if the source jitter  $\Delta t_{\text{Source}}$  is greater than the detector jitter  $\Delta t_{\text{Detector}}$ , the source jitter (determined from the photoluminescence lifetime – which can be a fraction of a nanosecond) should be used to calculate the signal-to-noise ratio in equation (2). The accumulation rate of coincidences in the  $g^{(2)}(\tau)$  histogram will depend not just on square of the detection efficiency and the frequency, but also on the brightness of the source [24].

QD SPS Wavelength (nm)	Detector	Detection efficiency ( $\eta$ )	Dark Count rate (Hz)	Jitter $\Delta t_{\text{Detector}}$ (ps)	Clock frequency(MHz)	Signal to Noise Ratio
~900	SNSPD (at 830 nm)	0.04	10	88	82	$4.55 \times 10^7$
		0.05	100	88	82	$5.7 \times 10^6$
		0.06	1000	88	82	$6.8 \times 10^5$
	Si SPAD (at 900 nm)	0.38	100	350	82	$1.1 \times 10^7$
~1310	SNSPD (at 1310 nm)	0.004	10	88	82	$4.55 \times 10^6$
		0.01	100	88	82	$1.1 \times 10^6$
		0.022	1000	88	82	$2.5 \times 10^5$
	InGaAs SPAD * (at 1310 nm)	0.09	234	260	1	$1.5 \times 10^6$

**Table 2:** Performance characteristics for candidate single-photon detectors in quantum-dot single-photon source (QD SPS) characterization experiments at 900 nm and 1310 nm wavelength. The SNSPD data is for Channel A of our system (see Figure 6). \*For the InGaAs SPAD,  $\eta$  and D are quoted/deduced from Refs. [5 & 28],  $\Delta t_{\text{Detector}}$  is quoted from Ref [29].

For QD SPS characterization at  $\lambda \sim 900$  nm, both Si SPADs and SNSPDs offer free-running operation and an excellent signal to noise ratio. The lower jitter of the SNSPD (88 ps FWHM) will allow a more accurate determination of the photoluminescence lifetime of the source. For a  $g^{(2)}(0)$  measurement, the Si SPAD has higher efficiency and will allow faster recording of coincidences.

For QD SPS characterization at  $\lambda \sim 1310$  nm, the main alternative to the SNSPD is the InGaAs SPAD. InGaAs SPADs offer detection efficiency  $\sim 10\%$  but with typically much higher dark count rates than SNSPDs, making gated operation essential [3]. By cooling the InGaAs SPAD to 165 K [5,27,28], low dark count rates can be achieved (as low as 230 Hz for a 3.5 ns gate [27]). However, operating the InGaAs SPAD at low temperature increases the afterpulsing probability, requiring a long dead time (up to 150 ms [3]). This means that the InGaAs SPAD can only be operated at a reduced clock rate (1 MHz), which reduces the overall coincidence accumulation rate dramatically. Therefore the SNSPD is the most versatile detector for the  $\lambda \sim 1310$  nm wavelength range; the low jitter and excellent signal-to-noise ratio will enable an accurate photoluminescence lifetime measurement and the free-running operation will enable fast  $g^{(2)}(0)$  measurements.

## 5. SUMMARY AND FUTURE WORK

In this paper we have described the construction and characterization of a superconducting nanowire single-photon detector (SNSPD) system designed for use in photon-counting experiments at wavelengths beyond 1  $\mu\text{m}$ . The detector performance is characterized in terms of detection efficiency, dark-count rate and timing jitter. We achieve greater than 1 % detection efficiency at  $\lambda = 1310$  nm in both SNSPD channels at a dark-count rate of 100 Hz. The FWHM timing jitter of both channels is less than 90 ps. This system is an important upgrade to the suite of single-photon detector facilities at the UK National Physical Laboratory (NPL). This system will be used in the characterization of single-photon sources emitting at  $\lambda \sim 1310$  nm and will allow more ambitious QIST and metrology experiments using telecom wavelength single-photon sources.

### Acknowledgements

This work was funded by the UK National Measurement System, and is supported by EPSRC and NPL via the Engineering Doctorate Scheme. Part of this work is also part of a EURAMET joint research project that receives funding from the European Community's Seventh Framework Programme, ERA-NET Plus, under Grant Agreement No. 217257. RHH acknowledges a Royal Society University Research Fellowship.

© Queen's Printer and Controller of HMSO, 2010

### References

- [1] Nielsen, M. A. and Chuang, I. L., "Quantum computation and quantum information", Cambridge (2000)
- [2] Shields, A. J., "Semiconductor quantum light sources", *Nature Photonics* 1, 215-223 (2007)
- [3] Hadfield, R. H., "Single-photon detectors for optical quantum information applications", *Nature Photonics* 3, 696-705 (2009)
- [4] Knill, E., Laflamme, R. and Milburn, G. J., "A scheme for efficient quantum computation with linear optics", *Nature* 409, 46-52 (2001)
- [5] Ward, M. B., Karimov, O. Z., Unitt, D. C., Yuan, Z. L., See, P., Gevaux, D. G., Shields, A. J., Atkinson, P., Ritchie, D. A., "On-demand single-photon source for 1.3  $\mu\text{m}$  telecom fibre", *Applied Physics Letters* 86(20), 201111 (2005)
- [6] Cova, S., Ghioni, M., Zappa, F., Rech, I., Gulinati, A., Maccagnani, P., "Evolution and prospects for single-photon avalanche diodes and quenching circuits", *Journal of Modern Optics* 51(9-10), 1267-1288 (2004)
- [7] Pellegrini, S., Warburton R. E., Tan, L. J. J., Ng, J. S., Krysa, A., Groom, K., David, J. P. R., Cova, S. D., Robertson, M. J., Buller, G. S., "Design and performance of an InGaAs/InP single-photon avalanche diode detector", *IEEE Journal of Quantum Electronics* 42(4), 397-403 (2006)
- [8] Gol'tsman G. N., Okunev, O., Chulkova, G., Lipatov, A., Semenov, A., Smimov, K., Voronov, B., Dzardanov, A., Williams, C., and Sobolewski, R., "Picosecond superconducting single-photon optical detector", *Applied Physics Letters* 79(6), 705-707 (2001)
- [9] Hadfield, R. H., Stevens, M. J., Gruber, S. S., Miller, A. J., Schwall, R. E., Mirin, R. P. and Nam, S. W., "Single photon source characterization with a superconducting single photon detector", *Optics Express* 13(26), 10846-10853 (2005)
- [10] Korneev, A., Matvienko, V., Minaeva, O., Milostnaya, I., Rubtsova, I., Chulkova, G., Smirnov, K., Voronov, V., Gol'tsman, G., Slysz, W., Pearlman, A., Verevkin, A. and Sobolewski, R., "Quantum efficiency and noise equivalent power of nanostructured, NbN, single-photon detectors in the wavelength range from visible to infrared", *IEEE Transactions on Applied Superconductivity* 15(2), 571-574 (2005)

- [11] Verevkin, A., Zhang, J., Sobolewski, R., Lipatov, A., Okunev, O., Chuikova, G., Korneev, A., Smirnov, K., Gol'tsman, G. N. and Semenov, A., "Detection efficiency of large-active-area NbN single-photon superconducting detectors in the ultraviolet to near-infrared range", *Applied Physics Letters* 80(25), 4687-4689 (2002)
- [12] Miki, S., Fujiwara, M., Sasaki, M., Baek, B., Miller, A. J., Hadfield, R. H., Nam, S. W. and Wang, Z., "Large sensitive-area NbN nanowire superconducting single-photon detectors fabricated on single-crystal MgO substrates", *Applied Physics Letters* 92(6), 061116 (2008)
- [13] Rosfjord, K. M., Yang, J. K. W., Dauler, E. A., Kerman, A. J., Anant, V., Voronov, B. M., Gol'tsman, G. N. and Berggren, K. K., "Nanowire single-photon detector with an integrated optical cavity and anti-reflection coating", *Optics Express* 14(2), 527-534 (2006)
- [14] Miki, S., Takeda, M., Fujiwara, M., Sasaki, M. and Wang, Z., "Compactly packaged superconducting nanowire single-photon detector with an optical cavity for multichannel system", *Optics Express* 17(26), 23557-23564 (2009)
- [15] Natarajan, C. M., Haertig, M., Warburton, R. E., Buller, G. S., Hadfield, R. H., Baek, B., Nam, S., Miki, S., Fujiwara, M., Sasaki, M., Wang, Z., [Quantum Communication and Quantum Networking], Springer, pp235-232 (2010)
- [16] Kerman, A. J., Dauler, E. A., Yang, J. K. W., Rosfjord, K. M., Anant, V., Berggren, K. K., Gol'tsman, G. N. and Voronov, B. M., "Constriction-limited detection efficiency of superconducting nanowire single-photon detectors", *Applied Physics Letters* 90(10), 101110 (2007)
- [17] Hadfield, R. H., Dalgarno, P. A., O'Connor, J. A., Ramsay, E., Warburton, R. J., Gansen, E. J., Baek, B., Stevens, M. J., Mirin, R. P., Nam, S. W., "Submicrometer photoresponse mapping of nanowire superconducting single-photon detectors", *Applied Physics Letters* 91(24), 241108 (2007)
- [18] Oxborrow, M. and Sinclair, A. G., "Single-photon sources", *Contemporary Physics* 46(3), 173-206 (2005)
- [19] Lounis, B. and Orrit, M., "Single-photon sources", *Reports on Progress in Physics* 68(5), 1129-1179 (2005)
- [20] Michler, P., Kiraz, A., Becher, C., Schoenfeld, W. V., Petroff, P. M., Zhang, L., Hu, E. and Imamoglu, A., "A quantum dot single-photon turnstile device", *Science* 290(5500), 2282-2285 (2000)
- [21] Keller, M., Lange, B., Hayasaka, K., Lange, W. and Walther, H., "Continuous generation of single photons with controlled waveform in an ion-trap cavity system", *Nature* 431, 1075-1078 (2004)
- [22] Beveratos, A., Brouri, R., Gacoin, T., Poizat, J. P. and Grangier, P., "Nonclassical radiation from diamond nanocrystals", *Physical Review A* 64, 061802(R) (2001)
- [23] Zinoni, C., Alloing, B., Li, L. H., Marsili, F., Fiore, A., Lunghi, L., Geradino, A., Yakhtomin, Y. B., Smirnov, K. V. and Gol'tsman, G. N., "Single-photon experiments at telecommunication wavelengths using nanowire superconducting detectors", *Applied Physics Letters* 91(3), 031106 (2007)
- [24] Hadfield, R. H., Stevens, M. J., Mirin, R. P. and Nam, S. W., "Single-photon source characterization with twin infrared-sensitive superconducting single-photon detectors", *Journal of Applied Physics* 101, 103104 (2007)
- [25] Bennett, A. J., Unitt, D. C., Atkinson, P., Ritchie, D. A. and Shields, A. J., "High-efficiency single-photon sources based on InAs/GaAs quantum dots in pillar microcavities", *Physica E* 26(1-4), 391-394 (2005)
- [26] Hanbury Brown, R. and Twiss, R. Q., "Interferometry of the Intensity Fluctuations in Light. I. Basic Theory: The Correlation between Photons in Coherent Beams of Radiation", *Proceedings of the Royal Society of London A* 242, 300-324 (1957)
- [27] Intallura, P. M., Ward, M. B., Karimov, O. Z., Yuan, Z. L., See, P., Shields, A. J., Atkinson, P. and Ritchie, D. A., "Quantum key distribution using a triggered quantum dot source emitting near 1.3  $\mu\text{m}$ ", *Applied Physics Letters* 91, 161103 (2007)
- [28] Intallura, P. M., "Quantum communication with a single photon source", PhD Thesis, University of Cambridge, (2010)